Quantum critical nature of the short-range magnetic order in $Sr_{2-x}La_xIrO_4$

Steven T. Rodan, Sungwon Yoon, Suheon Lee, and Kwang-Yong Choi*
Department of Physics, Chung-Ang University, Seoul, 06974, Republic of Korea

Gareoung Kim and Jong-Soo Rhyee
Department of Applied Physics, Kyung Hee University, Yongin, 17104, Republic of Korea

Akihiro Koda
Muon Science Laboratory, Institute of Materials Structure Science, High Energy Accelerator Research Organization (KEK), Tokai, Naka, Ibaraki, 319-1106 Japan

Wei-Tin Chen
Center for Condensed Matter Sciences, National Taiwan University, Taipei 10617, Taiwan

Fangcheng Chou
Center for Condensed Matter Sciences, National Taiwan University, Taipei 10617, Taiwan;
National Synchrotron Radiation Research Center, Hsinchu 30076, Taiwan;
and Taiwan Consortium of Emergent Crystalline Materials, Ministry of Science and Technology, Taipei 10622, Taiwan

(Received 19 July 2018; revised manuscript received 19 November 2018; published 10 December 2018)

We have investigated the nature of the short-range magnetic phase region of $Sr_{2-x}La_xIrO_4$ ($0 \leqslant x \leqslant 0.14$). This so-called spin-orbit Mott insulator's predicted transition to superconductivity with electron doping has remained elusive. Instead, short-range magnetism prevails over an extensive doping range up to the La solubility limit. We find evidence for quantum critical-like fluctuations of the short-range magnetic phase, in both a scaling relation of the ac susceptibility χT^{α} and the magnetization $MT^{\alpha-1}$ with $\alpha = 0.4$–0.5, as well as in the time-field scaling (t/H^{γ}) of the μSR asymmetry function. Our combined study of ac susceptibility and μSR, on the one hand, uncovers a two-stage weak symmetry breaking to spin freezing or proximate spin glass and to a subsequent spin glass within the short-range magnetic phase. On the other hand, we demonstrate that magnetic correlations become more static above $x = 0.06$ in spite of an apparent dilution of magnetic moments, indicative of enhanced inhomogeneities in a higher La-doping regime.

DOI: 10.1103/PhysRevB.98.214412

I. INTRODUCTION

Understanding the underlying mechanisms that govern the evolution of phases from long-range ordered magnetic insulators to high-temperature superconductors upon charge carrier doping in myriad correlated electron systems remains an attractive challenge within the condensed matter community. In the last decade, a surge of energy has also been put into investigating 5*d* iridate compounds owing to novel phenomena emerging from their strong spin-orbit coupling [1]. In particular, the single-layered perovskite Sr_2IrO_4 has garnered a lot of attention as it is the first spin-orbit Mott insulator identified [2].

The electronic and magnetic ground state properties were originally modeled after the $J_{\text{eff}} = 1/2$ isotropic Heisenberg model [3,4]. However, since then, anisotropic magnetic interactions have been observed in various experiments [5–7]. It was also predicted that superconductivity could potentially be induced via electron doping, just as in the hole-doped cuprates [8,9]. Angle-resolved photoemission spectroscopy (ARPES) and scanning tunneling microscopy/spectroscopy experiments probing surface-doped Sr_2IrO_4 have found *d*-wave pseudogap analogous to that seen in the cuprates [10,11]. However, bulk superconductivity signatures remain elusive, except for one ARPES study which reported an unusual metallic state with coherent nodal excitations and an antinodal pseudogap [12], but this is still not conclusive evidence.

Basic characterizations on the La substitution of Sr—including resistivity, dc and ac magnetization, and magnetotransport—have revealed an onset of spin-glass-like states at low temperatures from a metallic state [13]. Recent resonant inelastic x-ray scattering (RIXS) spectra have shown paramagnon excitations persisting deep into the metallic phase (up to $x = 0.1$), indicating short-range magnetic order far into the metallic phase, again analogous to hole-doped La_2CuO_4 [14]. Raman spectroscopy experiments have also seen clear pseudospin excitations detected well into the metallic regime beyond the disappearance of long-range order [15].

There is a large degree of general consistency among groups reporting on the phase diagram of $Sr_{2-x}La_xIrO_4$, e.g., with the loss of canted antiferromagnetic (CAF) long-range

*kchoi@cau.ac.kr

order around $x = 0.02$–0.04 [13,14]. But the detailed nature of the short-range magnetic region, and its associated inhomogeneous magnetism and competing order, has yet to be fully resolved.

Muon spin relaxation (μSR) is one of the ideal techniques in the physicist's toolkit to investigate microscopic, inhomogeneous magnetism due to its extreme sensitivity to very small magnetic moments. The first μSR study on a compound from this series ($x = 0.1$) was recently published and provided an indication to the formation of a spin-glass state [16]. Complementary to μSR, we further employ ac susceptibility towards unraveling a spatiotemporal structure of the short-range ordered spins.

In this paper, we report on a combined ac susceptibility (χ_{ac}) and μSR study on a series of electron-doped $Sr_{2-x}La_xIrO_4$ ($x = 0.01$, 0.02, 0.04, 0.06, 0.1, and 0.14). We find that short-range correlated spins undergo a symmetry breaking to a spin-glass state through spin freezing. In addition, the H dependence of $\chi_{ac}(T)$ along with the T dependence of dc magnetization $M(H)$ and a time-field μSR asymmetry separately revealed dynamic scaling behavior. These findings suggest that the short-range correlated spins may attain a quantum critical nature.

II. EXPERIMENTAL DETAILS

Polycrystalline samples of $Sr_{2-x}La_xIrO_4$ of various stoichiometries ($x = 0$, 0.01, 0.02, 0.04, 0.06, 0.1, and 0.14) were prepared by conventional solid state reaction method. Stoichiometric amounts of $SrCO_3$, La_2O_3, and IrO_2 thoroughly ground in an agate mortar and then calcinated at 1000 °C in air for 24 hours. Subsequently, powders were carefully reground and sintered again at 1100 ° and then 1200 °C to achieve a homogeneous single phase. Structural characterization by powder x-ray diffraction (XRD) was then performed using a Bruker D8 Advance diffractometer equipped with Cu Kα radiation. The lattice parameters were extracted by way of Rietveld refinement on the XRD data using the FullProf package [17] with crystallographic data taken from the Inorganic Crystal Structure Database [18].

Dc and ac magnetic susceptibilities were measured using a superconducting quantum interference device magnetometer and a vibrating sample magnetometer (Quantum Design MPMS and VSM). The magnetization measurements up to 14 T at various temperatures were carried out using a physical property measurement system (Quantum Design PPMS Dynacool).

Zero-field (ZF)- and longitudinal-field (LF)-μSR experiments were carried out using the Advanced Research Targeted Experimental Muon Instrument on the S line (ARTEMIS) spectrometer [19] at the Materials and Life Science Experimental Facility (MLF), J-PARC, Tokai, Japan. The collected data were fitted and analyzed using WiMDA software package [20]. For an overview on μSR with details regarding setup of experiments, see Refs. [21,22].

III. RESULTS AND DISCUSSION

A. Structural characterization

Figure 1(a) displays the powder XRD patterns of the $Sr_{2-x}La_xIrO_4$ ($x = 0$, 0.01, 0.02, 0.04, 0.06, 0.1, and 0.14). The patterns match well with that of tetragonal space group $I4_1/acd$ reported for Sr_2IrO_4. The samples appeared essentially pure, single-phased, with a small amount of impurity phase (<5%) of mostly La_2O_3, especially in the higher-doped samples. Figures 1(b) and 1(c) show the XRD patterns plotted with corresponding Rietveld refinements for the $x = 0$ and $x = 0.14$ samples. All other substitutions were similarly fitted to a degree of $\chi^2 \sim 1$. After sufficient fittings, we were able to extract the two lattice parameters a and c and plot their evolution with x while also comparing with the previously-reported values in Figs. 1(d) and 1(e), respectively [13,16,23]. Though the exact values don't overlap perfectly with those of any of the other groups, due to slight differences in synthesis conditions and preparation methods, they follow very similar trends. Most importantly, a increases slightly with La substitution while c decreases at a slightly greater rate until about $x = 0.1$, after which both values more or less appear to saturate. Consistent with each other, the La doping induces an expansion of the in-plane lattice constants accompanied by a reduction in the c-axis lattice parameter.

B. dc and ac magnetic susceptibility

We begin this section by presenting a magnetic phase diagram, based on the results presented in this paper. Previous reports [13,14,16,24] have unveiled a generic feature of the phase diagram of $Sr_{2-x}La_xIrO_4$; on doping 3–4% electrons, the long-range CAF order transits to the prominent short-range correlated phase, which survives up until the highest doped composition in this study of $x = 0.14$. The onset temperatures for short-range magnetic correlations in this diagram were taken from peaks in the second derivative of the dc magnetization with temperature. We will return to this diagram at the end after describing the various time-reversal symmetry breaking phases we were able to identify.

Figure 2(b) shows the temperature dependence of field-cooled (FC) dc magnetization for polycrystalline samples with $x = 0$, 0.01, 0.02, 0.04, 0.06, and 0.1. Higher La-doped samples' data were amplified for resolution and comparison, and the factors are shown in the figure. Our results generally follow similar line shapes of previously reported FC magnetization data, especially that of single crystal study by Chen *et al.* [13] (discrepancies in exact values likely due to different applied fields). Upon cooling below $T_N = 240$ K, $M(T)$ of the $x = 0$ and 0.01 samples exhibits a ferromagneticlike increase due to the formation of the CAF order. With increasing x above 0.02, the ferromagnetic response is strongly diminished. Instead, $M(T)$ displays a first steep increase down to 200 K, followed by a slope change at 100 K and then a small kink at 20 K.

Plotting on a double log scale in Fig. 2(c), we can clearly observe that $M(T)$ displays a power-law behavior in the intermediate-temperature region for $x \geqslant 0.04$, as seen by the solid black lines. For example, the $x = 0.1$ sample obeys $M(T) \propto T^{-\nu}$ with $\nu = 0.4 \pm 0.05$ in the temperature range of $T = 10$–100 K. We stress that the power dependence of $M(T)$ observed in the limited temperature interval alone is not sufficient to conclude the presence of critical spin dynamics. Rather, it motivates us to examine whether the short-range correlated spins acquire a quantum critical nature

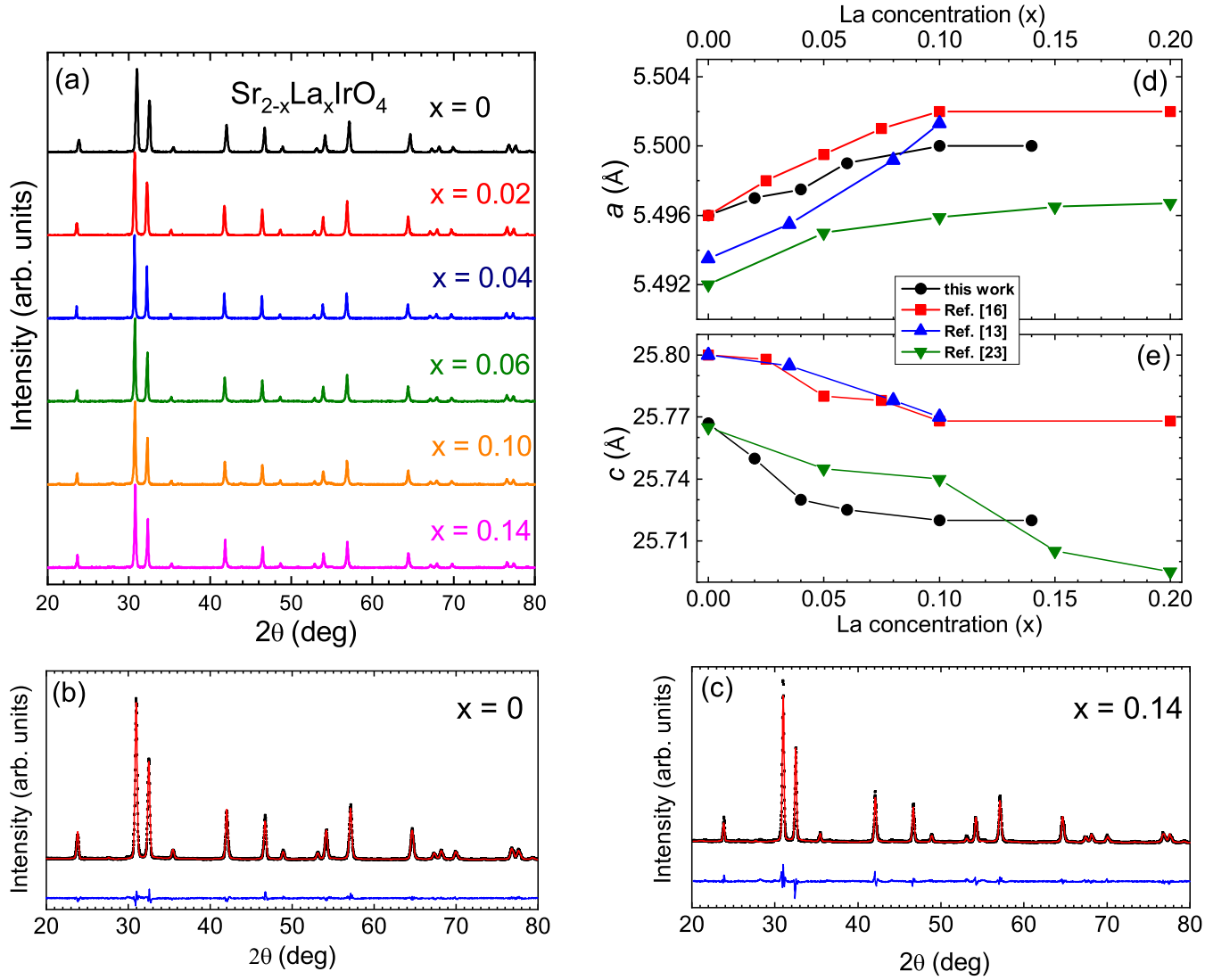

FIG. 1. (a) X-ray diffraction pattern of $Sr_{2-x}La_xIrO_4$ with La concentrations in a range of $x = 0$–0.14. Representative examples of the Rietveld refinement results for (b) $x = 0$ and (c) $x = 0.14$. The x dependence of the lattice parameters a and c extracted from the refinements are plotted in (d) and (e) and compared with previous reports.

in a higher-doped regime. To substantiate dynamic scaling, we performed ac susceptibility (χ_{AC}) on several compositions, with an emphasis on $x = 0.1$.

Figure 2(d) shows the real part of the zero-field ac susceptibility of $x = 0.01$, 0.04, 0.06, and 0.1, measured with 100 Hz frequency and 10 Oe oscillating field. A sharp peak, indicative of a long-range CAF phase transition, is seen around $T_N = 230$ K at $x = 0.01$ but not for the others. Instead, the higher-doped samples ($x > 0.04$) show first a broad maximum and then the second hump around 11–17 K, followed by a steep decrease to zero susceptibility, typical of spin-glass-like transitions. This together with the splitting between FC and ZFC magnetization (not shown here) suggests the successive occurrence of weak time-reversal symmetry breaking. Here we further note that the monotonic decrease in the higher-T peak positions for $x = 0.04$ at $T_f = 100$ K to 80 K for $x = 0.06$ was expected, but the increase for $x = 0.1$ was unexpected and likely due to stronger inhomogeneity or phase segregation which could enhance spin glassiness. Because of this the $x = 0.04$ and 0.1 samples were selected for a further comparative investigation into the frequency dependence of their peaks.

Figures 3(a) and 3(b) show the temperature dependence of the in-phase component of χ'_{AC} measured over the frequency range 2–300 Hz, for $x = 0.04$ and $x = 0.1$, respectively. The two distinct peaks were observed at all frequencies, with the dominant high-temperature peak at $x = 0.1$, found at 120 K (at 2 Hz), showing a slight, though clear frequency dependence, while the corresponding peak in $x = 0.04$, along with the low-temperature smaller peaks, displays no such discernible shift with changing frequency. Like canonical spin glasses, with increasing frequency this peak decreases in magnitude and shifts to higher temperatures. The position of this peak in χ'_{AC} was taken as a freezing/blocking temperature (T_f).

To check the nature of the frequency dependence, we calculated the fractional relative change in T_f with respect to decade change in frequency (ν), sometimes denoted by ϕ and

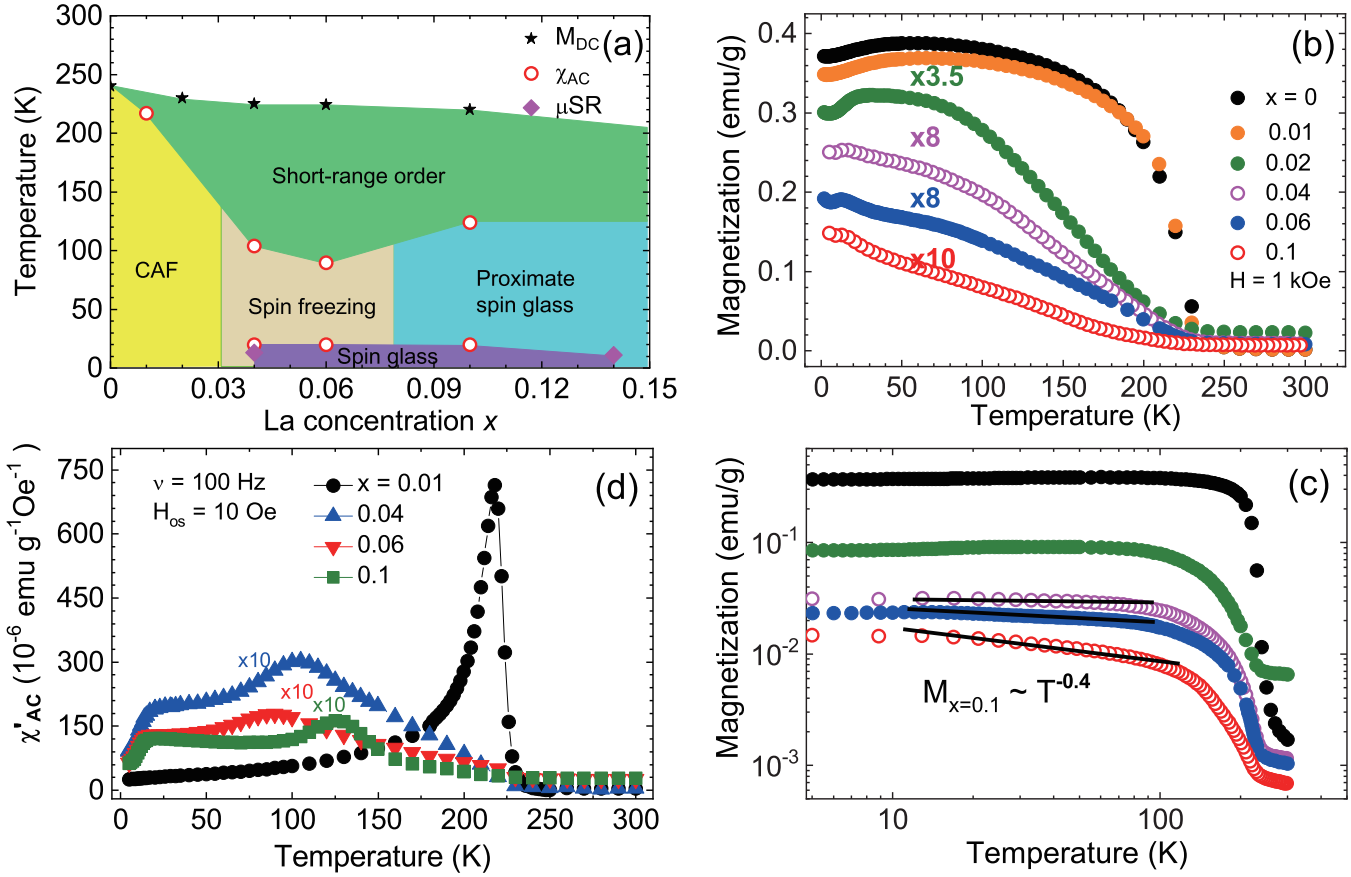

FIG. 2. (a) $T - x$ phase diagram of $Sr_{2-x}La_xIrO_4$. The phase boundaries of the long-range canted antiferromagnetic (CAF), short-range magnetic, spin freezing, and (proximate) spin glass regions are determined by the dc magnetization, ac magnetic susceptibility and μSR. (b) Temperature dependence of the dc magnetization measured with an applied field of $H = 1$ kOe for $x = 0$, 0.01, 0.02, 0.04, 0.06, and 0.1. (c) The same magnetization plotted on a log-log scale to clearly see its power-law dependence. The solid dark lines are a power-law fit $M(T) \sim T^{-\nu}$ with $\nu = 0.4$ at $x = 0.1$ between 10 and 100 K. (d) Temperature dependence of the ac magnetic susceptibility for selected compositions measured in a 100 Hz frequency and an oscillating field of 10 Oe.

written as

$$\phi = \frac{\Delta T_f}{T_f \Delta \log_{10}(\nu)}, \tag{1}$$

where standard spin glasses typically have a ϕ value around 0.005–0.05 [25]. In Fig. 3(c) we plot fittings of the data with Eq. (1) for the $x = 0.04$ and 0.1. The $x = 0.04$ sample indeed shows practically no shift at all, while for the $x = 0.1$ sample $\phi = 0.007(1)$, which falls within the range of conventional spin glass systems, especially similar to the prototypical spin glass CuMn ($\phi = 0.005$) [26]. While the magnitude of the peak does decrease with increasing frequency, the absence of any discernible shift in the $x = 0.04$ case means that there is spin freezing occurring around $T_f = 104$ K.

Based on the dc magnetization results shown in Fig. 2(b), we also checked the field dependence of the $x = 0.1$ sample in an attempt to search for further evidence of dynamic scaling behavior. Figure 4(a) shows the H and T dependences of χ'_{AC} for $x = 0.1$ with applied dc fields in the range of $\mu_0 H =$ 0.1–3 T. With increasing field, $\chi'_{AC}(T)$ is systematically reduced. In Fig. 4(b) we analyzed these results for critical scaling behavior by plotting $\chi'_{AC} T^{\alpha}$ vs $\mu_B H / k_B T$ [27]. Remarkably, the data overlap most completely for $\alpha = 0.4 \pm 0.05$, so already we see some hint to universal scaling behavior, which has been associated with the existence of quantum critical fluctuations in, for example, quantum antiferromagnets [28] and heavy fermion systems [29]. Further supportive evidence for this interpretation comes from checking the similar scaling behavior in the field dependence of $M(H)$ measured up to $\mu_0 H = 14$ T at various temperatures ($T = 2$, 3, 4, 5, 12, and 20 K) [27]. We plot $MT^{\alpha-1}$ against $\mu_B H / k_B T$ in Fig. 4(c) and find that the exponent value needed for a similarly sufficient data overlap corresponds to $\alpha = 0.5 \pm 0.05$. Within the error bars, thus, the critical exponent value agrees quite well between the independent dc and ac methods with $\alpha =$ 0.4–0.5, indicating that there are spins with either fluctuations close to quantum critical nature or random interactions. As to a random singlet, χ'_{AC} does not exhibit a suppression of the low-T dynamic response up to $\mu_0 H = 3$ T [see Fig. 4(a)], rendering the random-singlet scenario improbable.

C. ZF- and LF-μSR

Figures 5(a) and 5(b) show the ZF-μSR spectra of the $x =$ 0.04 and 0.14 samples, at a range of selected temperatures from near room temperature down to 4 K. The clear lack of any sinusoidal oscillatory signal in any spectrum indicates an absence of long-range magnetic order, consistent with our

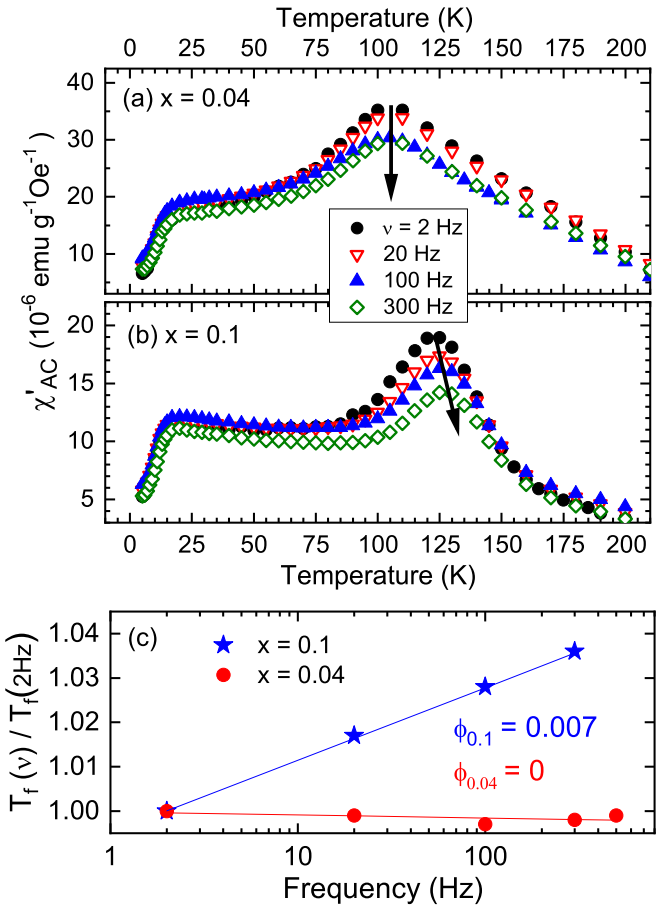

FIG. 3. Temperature dependence of the ac magnetic susceptibility plotted for various frequencies from 2 to 300 Hz, for (a) the $x = 0.04$ and (b) the $x = 0.1$ samples. The oscillating field was 10 Oe at zero dc field. (c) The change in relative freezing temperature with respect to change in frequency, plotted with the ratio $T_f/T_f(2\ \mathrm{Hz})$ as the y-axis, and frequency on a log scale as the x-axis. The solid lines are linear fits to the data.

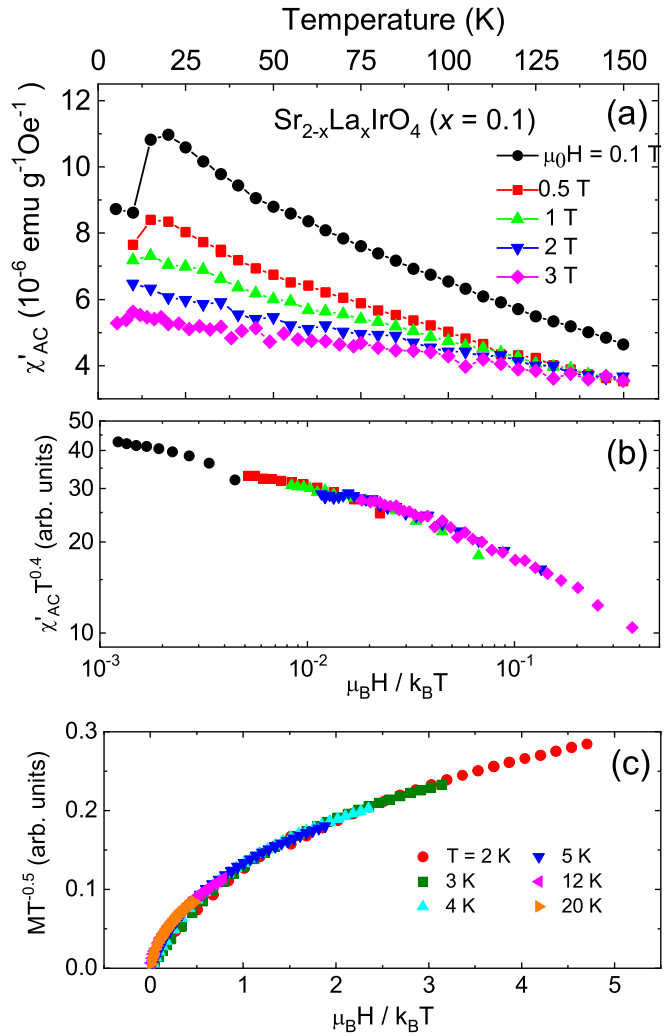

FIG. 4. (a) The in-phase component of the ac magnetic susceptibility plotted against temperature for $x = 0.1$, measured in various applied dc fields. The frequency was fixed at 100 Hz and the oscillating field was 10 Oe. (b) Log-log scaled plot of the ac susceptibility, displayed as $\chi'_{AC}T^{\alpha}$ with $\alpha = 0.4$ on the y axis and $\mu_B H/k_B T$ on the x axis. (c) dc magnetization plotted as $MT^{-0.5}$ vs $\mu_B H/k_B T$.

magnetization results. At first glance, the spectra of these different La dopings appear almost identical, yet there are some notable differences.

As seen in Fig. 5(a), the room-temperature ZF-μSR of $x = 0.04$ shows an exponential-like slow muon spin relaxation caused by rapidly fluctuating dynamical fields of Ir moments. As the temperature is further lowered, the depolarization increases appreciably, pointing to a development of short-range magnetic correlations. On the other hand, a close look at Fig. 5(b) near room temperature uncovers that the ZF-μSR spectrum of $x = 0.14$ is approximated by a Gaussian-like relaxation [see also the open squares in Fig. 6(b)], implying that the muon depolarization is dominated by a static distribution of random local magnetic fields mainly from nuclear magnetic moments. With the amount of La doping, the $x = 0.14$ sample is in the more dilute region than the $x = 0.04$ sample, where it would make sense for the muons to feel the nuclear moments, normally screened by the electrons in less-dilute regimes.

The shallow dip visible from 11 K in both samples indicates the formation of quasistatic internal fields [30]. This time-reversal symmetry breaking occurs between 15 and 11 K, which agrees with the onset temperature of a rapidly dropping low-T $\chi'_{AC}(T)$ [see Fig. 2(d) and Figs. 3(a) and 3(b)]. For both samples, thus, the μSR spectrum analysis can be divided into high and low-temperature regimes, where different polarization functions G(t) were used to fit and extract parameters relevant to the local spin states.

At $T = 4$ (4.8) K of $x = 0.04$ (0.14), the muon polarization does recover to almost 1/3 the initial asymmetry just after the dip, while decreasing slowly at intermediate times. This, together with the early-time rapid drop, suggests that a ground state of $Sr_{2-x}La_xIrO_4$ ($x > 0.04$) is characterized by quasistatic magnetism.

In order to separate or decouple the dynamic local field contribution from any static random fields felt by the muons, one can apply a longitudinal field (LF) parallel to the initial polarization of the muon spin momentum. With a strong enough applied field, one can eliminate any contribution of

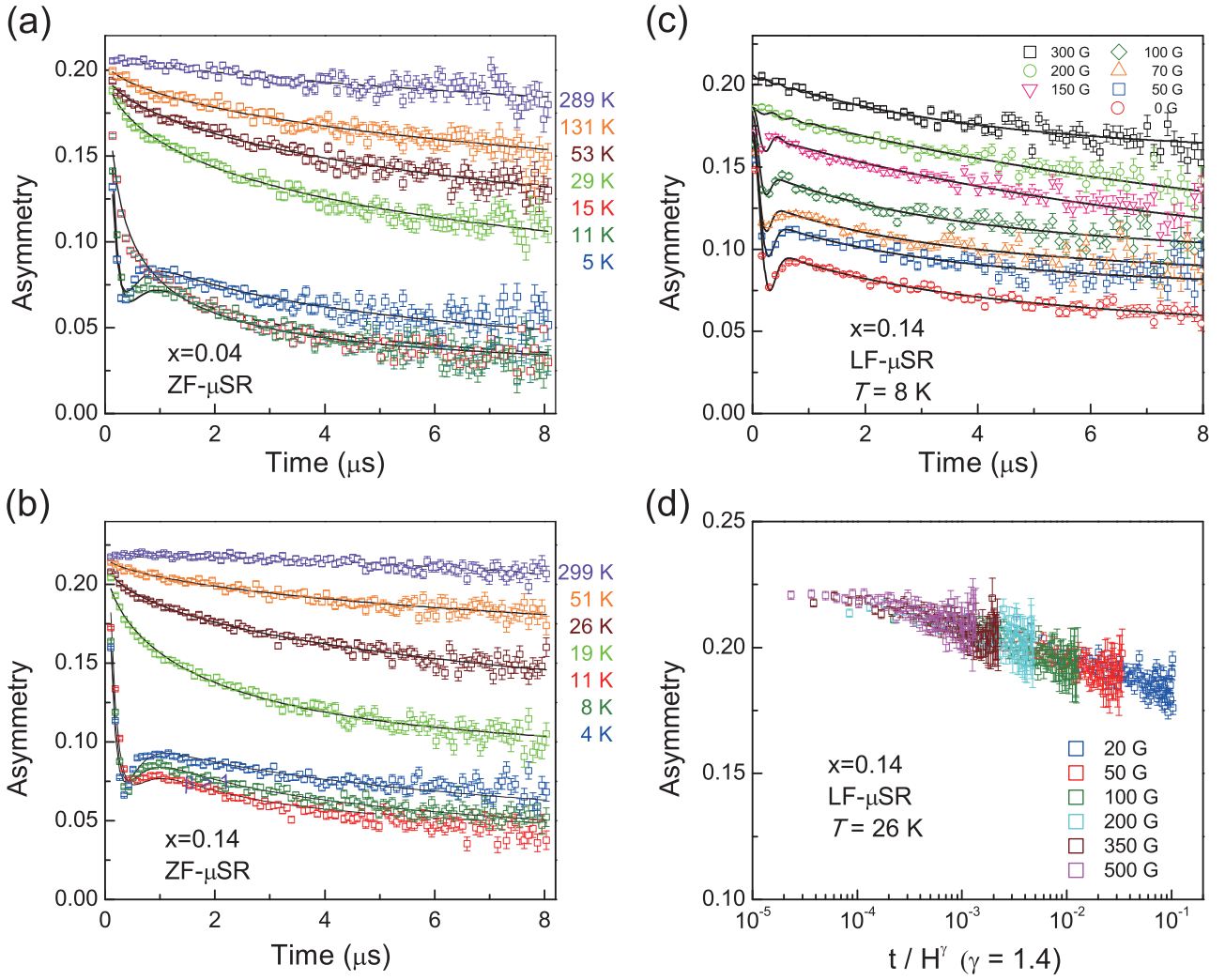

FIG. 5. ZF-μSR spectra measured at various temperatures are displayed for (a) $x = 0.04$ and (b) $x = 0.14$ samples. (c) LF-μSR on $x = 0.14$ measured in various fields (H = 0–300 G) at $T = 8$ K. (d) Time-field scaling of the depolarization at $T = 26$ K, with the asymmetry plotted on a log-normal scale against t/H^{γ} with $\gamma = 1.4$. The solid lines represent fits of the data as described in the main text.

static random fields and thus see a slow decay due to dynamic spin fluctuations.

Figure 5(c) shows the LF-μSR spectra of the $x = 0.14$ sample, measured at $T = 8$ K. The LF-μSR spectra display a systematic, upward shift with increasing field. Above $H = 200$ G, there remains an unquenched exponential-like relaxation [see also Figs. 7(e) and 7(f)]. This confirms a coexistence of the inhomogeneous quasistatic and dynamic magnetism. LF-μSR was also measured at $T = 26$ K in a similar range of H values, and Fig. 5(d) shows the LF-μSR asymmetry plotted against a time-field scaling (t/H^{γ}). At this temperature, we find that the LF-μSR data overlap over three orders of magnitude in t/H^{γ} with $\gamma = 1.4$. For the case of $\gamma = 1 + \beta > 1$, the dynamic spin-spin autocorrelation function, $q(t) = \langle \mathbf{S}(0) \cdot \mathbf{S}(t) \rangle$ is given by a stretched exponential spin-spin correlation function $q(t) \sim \exp[-(\lambda t)^{\beta}]$ [31,32]. The stretched spin-spin correlation with $\beta = 0.4$ is fully consistent with the ZF-μSR results showing the stretching exponent of $\beta = 0.44(3)$ [see below and Fig. 6(b)]. Thus, our μSR data lend further support to a quantum critical-like nature of the short-range ordered spins. For $T \geqslant 15$ K, the ZF-μSR spectra of the $x = 0.04$ and 0.14 samples are well fitted by the stretched exponential function, representative of disordered systems with broad distribution of the relaxation rates, expressed as

$$G_{ZF}(t) = (1 - A_{bg}) \exp[(-\lambda t)^{\beta}] + A_{bg}, \qquad (2)$$

where λ is the relaxation rate, β is the stretched exponent, and A_{bg} is the time-independent background due to muons which have stopped in the sample holder (rather than the sample itself).

Figure 6(a) shows the temperature dependence of $\lambda(T)$. It was plotted on a log-log scale in order to most easily see key differences between $x = 0.04$ and 0.14 samples. For both samples, $\lambda(T)$ starts to diverge as the temperature approaches the lowest temperatures where the asymmetry could be fitted well with Eq. (2), indicating a critical slowing down of the moment fluctuations. This makes sense as the appearance of the shallow dip (static moments) in low-temperature spectra occurs immediately below this point in temperature [see Figs. 5(a) and 5(b)]. However, the high-T behavior of $\lambda(T)$ is distinct between the two samples belonging to the same

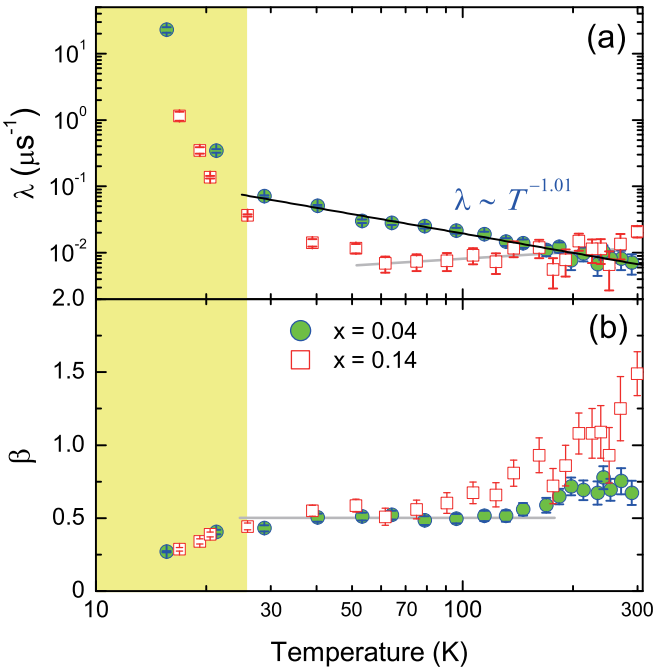

FIG. 6. Log-log plot of the relaxation rates λ vs temperature for the $x = 0.04$ (full green circles) and 0.14 samples (open red squares), obtained from stretched exponential fits. The thin solid line represents a fit to $\lambda(T) \sim T^{-1.01}$ and the thick gray lines are a guide to the eye. (b) Comparison of the stretching exponent values β between $x = 0.04$ and 0.14. The yellowish green shading marks a spin-glass state [see Fig. 2(a)].

short-range ordered state. The $x = 0.04$ sample clearly shows a power-law increase $T^{-1.01}$ on cooling from room temperature to 25 K, indicative of a weakly growing spin-spin correlation length with temperature. In contrast, $\lambda(T)$ of the $x = 0.14$ sample displays a weak decrease with decreasing temperature through $T = 200$ K [see the gray line in Fig. 6(a)]. This means that the more diluted sample has a stronger tendency to the frozen magnetic moments. This distinct behavior is reflected in the T dependence of the stretching exponent β as seen in Fig. 6(b). For $x = 0.14$, $\beta(T)$ continues to decrease from 1.5 at room temperature to 0.5 at 25 K. This is contrasted by $\beta(T)$ of $x = 0.04$, which undergoes a weak steplike drop from 0.7 to 0.5 on cooling down through $T = 160$ K. Then, from $T = 160$ K down to $T = 25$ K, $\beta(T)$ remains around 0.5, a value reportedly associated with a short-range magnetic Griffiths phase [16,33]. Both the $\lambda(T)$ and $\beta(T)$ in these compounds closely resemble those recently reported for the $x = 0.1$ polycrystalline sample [16]. As with that compound, $\beta(T)$ eventually converges on the value of 1/3 at the transition temperature (in these two samples) of 15 K ($x = 0.04$) and 11 K ($x = 0.14$). This has been shown to signify a spin-glass state [34,35] and is at the same temperature where $\lambda(T)$ diverges (see the color shading in Fig. 6).

Finally, we examine the low-T region in more detail, where a shallow dip signals the partial freezing of the fluctuating local fields into a spin glass state, contributing to the static field at the muon sites [30]. These temperatures ($T_{SG} = 13$ K in $x = 0.04$ and very similar $T_{SG} = 11$ K in $x = 0.14$) coincide with the second, smaller frequency-independent peaks of $x = 0.04$ and 0.1 in the χ'_{AC} seen in Figs. 3(a) and 3(b). From this temperature down to the lowest measured, we fit the ZF-μSR data with two different phenomenological models, which are suited to describe coexisting static and dynamic magnetism, well separated in a μSR time window. The first model is a dynamical Gaussian Kubo-Toyabe (DGKT) relaxation function supplemented with a time-independent background signal:

$$G(t) = A_{DGKT} G^{DGKT}(t, \Delta, \nu, H_{LF}) + A_{bg}, \tag{3}$$

where A_{DGKT} and A_{bg} are the asymmetries associated with the DGKT and background signals, respectively. The parameter Δ is the static width of the local fields at the muon sites and ν is the field fluctuation rate.The DGKT function is given by $G^{DGKT}(t) = G^{KT}(t)\exp(-\nu t) + \nu \int_0^t dt\{G^{DGKT}(t - t')G^{KT}(t')\exp(-\nu t')\}$ where the Gaussian Kubo-Toyabe relaxation function is defined by $G^{KT} = \frac{1}{3} + \frac{2}{3}(1 - \Delta^2 t^2)\exp(-\frac{1}{2}\Delta^2 t^2)$.

Next, we attempt to fit the low-T data to a so-called spin-glass model [30] given as

$$G_{ZF}(t) = \frac{1}{3}\exp(-\sqrt{\lambda_d t}) + \frac{2}{3}\left(1 - \frac{a_s^2 t^2}{\sqrt{\lambda_d t + a_s^2 t^2}}\right)\exp\left(-\sqrt{\lambda_d t + a_s^2 t^2}\right), \tag{4}$$

where λ_d and a_s represent the dynamic relaxation rate and the static field amplitude. We note that both models reproduce reasonably the characteristic features of the spectra but the DGKT model remains valid at slightly higher temperature than T_{SG} and allows analyzing the LF-μSR spectra. The fitting results are summarized in Fig. 7. Overall, a temperature evolution of the extracted parameters shows little difference between the two sets of fitting functions.

As the temperature is lowered from $T = 16$ K, for both $x = 0.04$ and 0.14, $\nu(T)$ and $\lambda_d(T)$ decrease continuously with no indication of flattening out [see Figs. 7(a) and 7(c)]. This points to a steady growth of the frozen spin state with decreasing temperature at least down to 4 K. The order-parameter-like decrease of the static component with increasing temperature is further evidenced by the T dependences of $\Delta(T)$ and $a_s(T)$ as shown in Figs. 7(b) and 7(d). Since $\Delta(T) \sim \nu(T)$ at $T = 15.5$ K, it is difficult to determine $\Delta(T)$ and $\nu(T)$ above 15.5 K in an unambiguous manner and thus we are not able to identify $\Delta(T) \approx 0$ at about 16 K. In Figs. 7(e) and 7(f), we show the H dependence of the fit parameters for $x = 0.14$ measured at $T = 8$ K. Both $\Delta(H)$ and $\nu(H)$ start to increase slightly with H and then decrease towards zero above 200 G. This means that the static component is mostly quenched through a spin-locking effect at $H \approx 200$ G, allowing an estimate of the local static field of 20 G (= one tenth of 200 G).

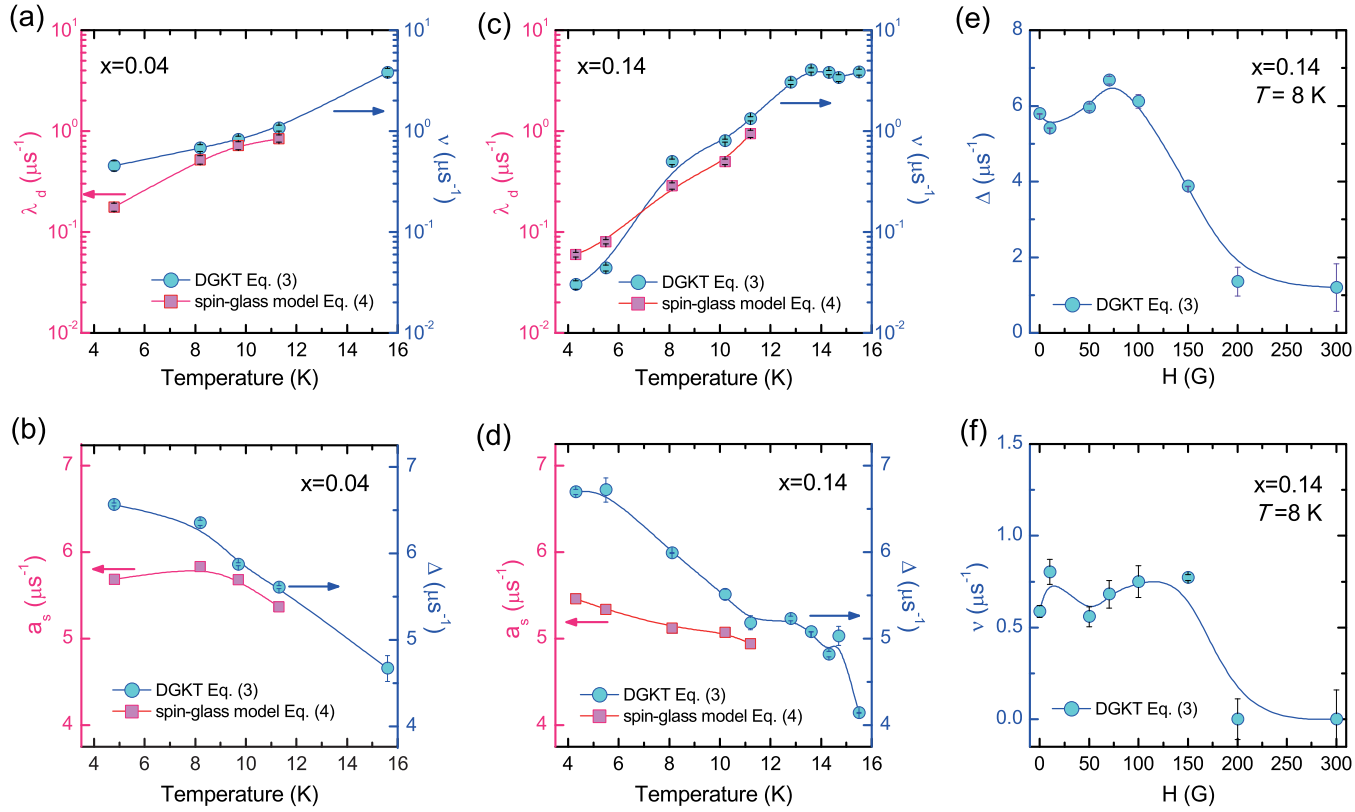

FIG. 7. Temperature dependence of the fluctuation rate (ν) and the dynamic relaxation rate (λ_d) for (a) $x = 0.04$ and (c) $x = 0.14$ obtained from fitting the ZF-μSR spectra to the DGKT and spin-glass models, respectively, described in the main text. Temperature dependence of the static field components (Δ and a_s) for (b) $x = 0.04$ and (d) $x = 0.14$. Longitudinal-field dependence of (e) $\Delta(H)$ and (f) $\nu(H)$ for $x = 0.14$ measured at $T = 8$ K. We note that the LF data were fitted only to the DGKT model.

IV. CONCLUSION

The different frequency ranges of χ_{AC} and μSR experiments allow one to probe different time windows of spin fluctuations and thus are complementary techniques. Using these in addition to dc magnetization we were able to add some details to identify weak broken symmetry phases, in the extensive short-range magnetically ordered region of $0.04 \leqslant x \leqslant 0.14$, shown in Fig. 2(a).

First, long-range order is already absent in $x = 0.04$, where instead we found a spin freezing around $T_f = 104$ K, seen in the χ'_{AC}. On the other hand, its peak at slightly higher 120 K in $x = 0.1$ signals a conventional spin glass freezing/blocking temperature, due to its frequency dependence being very similar to other classical spin glass systems. This is contrasted by the ZF-μSR results; for $x = 0.14$ the lacking sharp peak in $\lambda(T)$ and the stretching exponent bigger than $\beta = 1/3$ support spin freezing rather than spin glass (see Fig. 6). This apparent paradox implies that a spatiotemporal structure of the correlated spins in higher electron-doped regimes is strongly frequency dependent. In this regard, for $x > 0.06$ the intermediate-T phase occurring between T_{SG} and T_f is called a proximate spin glass for the distinction.

Upon lowering the temperature further, the $x = 0.04$, 0.1, and 0.14 samples undergo another time-reversal symmetry breaking transition into a spin-glass state below $T_{SG} =$ 11–13 K, which is seen as the presence of a static fraction of magnetic moments along with the second anomaly in low-T χ'_{AC}. The successive symmetry breaking can be understood in terms of nanoscale phase segregations consisting of metallic and insulating regions. With decreasing temperature, the spins first start to freeze out by forming antiferromagnetic nanoscale clusters and then above a percolation limit, a static fraction of frozen moments appears on a μSR time scale.

From combined dc and ac magnetization we found evidence of quantum critical fluctuations in $x = 0.1$ from fitting both χT^{α} and the magnetization $MT^{\alpha-1}$ as functions of dimensionless $\mu_B H/k_B T$ with $\alpha = 0.4$–0.5. A time-field scaling t/H^{γ} with $\gamma = 1.4$ over three orders of magnitude provided further evidence of quantum critical nature of spins in $x = 0.14$. Given the absence of an obvious quantum critical point, a random singlet or a Griffith phase may be also invoked to account for the observed scaling relation. Based on the fact that the χ'_{AC} data do not show an opening of a field-induced spin gap, we exclude a formation of the random singlet. The Griffiths phase usually emerges in the highly dilute regime, where strong magnetic correlations no longer exist. For the studied system, however, a RIXS study unveiled that the dispersive magnon excitations of undiminished spectral weight persist deep into the metallic part of the phase diagram (at least up to $x = 0.1$) [14]. The robust AFM fluctuations in the metallic phase are consistent with the prevailing short-range order. In addition, magnetic resonant X-ray scattering measurements evidenced that part of the short-range order transits into an incommensurate spin density wave state through $x =$ 0.08 [24]. These observations disfavor the Griffith phase. We

conjecture that a quantum critical point is hidden by disorders and inhomogeneities as seen by the enhanced spin freezing across $x = 0.06$. A further support to this assertion is provided by the observation of a quantum critical phenomenology in the bilayer counterpart $(Sr_{1-x}La_x)_3Ir_2O_7$ [36]. However, we admit that future experimental work is needed for ultimate corroboration of the putative quantum criticality.

The surprising enhancement of (short-range) magnetism for $x > 0.06$, rather than a suppression, is unexpected and is believed to not be an intrinsic effect of this system. Rather, our results suggest that a degree of disorders, including magnetic inhomogeneity or phase segregation, becomes larger in the higher-doped compounds as a result of oxygen deficiency, which is often created near the La^{3+} substituted site to maintain the Ir^{4+} valence of d^5 half-filled particular stable. If a true bulk superconducting phase is to be unambiguously found in this system, it may require improved novel synthesis methods, such as increasing oxygen partial pressure in the growth atmosphere to reduced oxygen vacancies in the crystal structure. Despite an inhomogeneous disordered magnetism prevailing over an extended short-range correlated region, our finding of quantum scalings in frequency, time, and energy provides compelling evidence that the short-range correlated spins bear quantum critical dynamics, possibly heralding a neighboring superconducting phase.

ACKNOWLEDGMENTS

This work is supported by Korea Research Foundation (KRF) Grants (No. 2018-00999, No. 2018-0189, and No. 2018-0414). The muon experiment at the Materials and Life Science Experimental Facility (MLF) of J-PARC was performed under a user program (Proposal No. 2018A0143).

[1] G. Cao and P. Schlottmann, Rep. Prog. Phys. **81**, 042502 (2018).
[2] M. K. Crawford, M. A. Subramanian, R. L. Harlow, J. A. Fernandez-Baca, Z. R. Wang, and D. C. Johnston, Phys. Rev. B **49**, 9198 (1994).
[3] B. J. Kim, H. Jin, S. J. Moon, J.-Y. Kim, B.-G. Park, C. S. Leem, J. Yu, T. W. Noh, C. Kim, S.-J. Oh, J.-H. Park, V. Durairaj, G. Cao, and E. Rotenberg, Phys. Rev. Lett. **101**, 076402 (2008).
[4] B. J. Kim, H. Ohsumi, T. Komesu, S. Sakai, T. Morita, H. Takagi, and T. Arima, Science **323**, 1329 (2009).
[5] S. Bahr, A. Alfonsov, G. Jackeli, G. Khaliullin, A. Matsumoto, T. Takayama, H. Takagi, B. Büchner, and V. Kataev, Phys. Rev. B **89**, 180401(R) (2014).
[6] J. G. Vale, S. Boseggia, H. C. Walker, R. Springell, Z. Feng, E. C. Hunter, R. S. Perry, D. Prabhakaran, A. T. Boothroyd, S. P. Collins, H. M. Rønnow, and D. F. McMorrow, Phys. Rev.B **92**, 020406 (2015).
[7] Y. Gim, A. Sethi, Q. Zhao, J. F. Mitchell, G. Cao, and S. L. Cooper, Phys. Rev. B **93**, 024405 (2016).
[8] F. Wang and T. Senthil, Phys. Rev. Lett. **106**, 136402 (2011).
[9] Z. Y. Meng, Y. B. Kim, and H.-Y. Kee, Phys. Rev. Lett. **113**, 177003 (2014).
[10] Y. K. Kim, N. H. Sung, J. D. Denlinger, and B. J. Kim, Nat. Phys. **12**, 37 (2016).
[11] Y. J. Yan, M. Q. Ren, H. C. Xu, B. P. Xie, R. Tao, H. Y. Choi, N. Lee, Y. J. Choi, T. Zhang, and D. L. Feng, Phys. Rev. X **5**, 041018 (2015).
[12] A. de la Torre, S. McKeown Walker, F. Y. Bruno, S. Riccó, Z. Wang, I. Gutierrez Lezama, G. Scheerer, G. Giriat, D. Jaccard, C. Berthod, T. K. Kim, M. Hoesch, E. C. Hunter, R. S. Perry, A. Tamai, and F. Baumberger, Phys. Rev. Lett. **115**, 176402 (2015).
[13] X. Chen, T. Hogan, D. Walkup, W. Zhou, M. Pokharel, M. Yao, W. Tian, T. Z. Ward, Y. Zhao, D. Parshall, C. Opeil, J. W. Lynn, V. Madhavan, and S. D. Wilson, Phys. Rev. B **92**, 075125 (2015).
[14] H. Gretarsson, N. H. Sung, J. Porras, J. Bertinshaw, C. Dietl, J. A. N. Bruin, A. F. Bangura, Y. K. Kim, R. Dinnebier, J. Kim, A. Al-Zein, M. Moretti Sala, M. Krisch, M. Le Tacon, B. Keimer, and B. J. Kim, Phys. Rev. Lett. **117**, 107001 (2016).
[15] H. Gretarsson, J. Sauceda, N. H. Sung, M. Hoppner, M. Minola, B. J. Kim, B. Keimer, and M. Le Tacon, Phys. Rev. B **96**, 115138 (2017).
[16] K. Horigane, M. Fujii, H. Okabe, K. Kobayashi, R. Horie, H. Ishii, Y. F. Liao, Y. Kubozono, A. Koda, R. Kadono, and J. Akimitsu, Phys. Rev. B **97**, 064425 (2018).
[17] J. Rodriguez-Carvajal, Physica B **192**, 55 (1993).
[18] Q. Huang, J. L. Soubeyroux, O. Chmaissem, I. Natali Sora, A. Santoro, R. J. Cava, J. J. Krajewski, and W. F. Peck, Jr., J. Solid State Chem. **112**, 355 (1994).
[19] K. M. Kojima, T. Murakami, Y. Takahashi, H. Lee, S. Y. Suzuki, A. Koda, I. Yamauchi, M. Miyazaki, M. Hiraishi, H. Okabe, S. Takeshita, R. Kadono, T. Ito, W. Higemoto, S. Kanda, Y. Fukao, N. Saito, M. Saito, M. Ikeno, T. Uchida, and M. M. Tanaka, J. Phys. Conf. Ser. **551**, 012063 (2014).
[20] F. L. Pratt, Physica B **289-290**, 710 (2000).
[21] S. Blundell, Contemp. Phys. **40**, 175 (1999).
[22] S. L. Lee, S. H. Kilcoyne, and R. Cywinski, *Proc. Fifty First Scottish Universities Summer School in Physics, St. Andrews, August 1988* (Institute of Physics, New York, 1999).
[23] C. Cosio-Castaneda, G. Tavizon, A. Baeza, P. de la Mora, and R. Escudero, J. Phys.: Condens. Matter **19**, 446210 (2007).
[24] X. Chen, J. L. Schmehr, Z. Islam, Z. Porter, E. Zoghlin, K. Finkelstein, J. P. C. Ruff, and S. D. Wilson, Nat. Commun. **9**, 103 (2018).
[25] G. F. Goya and V. Sagredo, Phys. Rev. B **64**, 235208 (2001).
[26] J. A. Mydosh, *Spin Glasses: An Experimental Introduction* (Taylor & Francis, Washington, DC, 1993).
[27] J. S. Helton, K. Matan, M. P. Shores, E. A. Nytko, B. M. Bartlett, Y. Qiu, D. G. Nocera, and Y. S. Lee, Phys. Rev. Lett. **104**, 147201 (2010).
[28] S. Sachdev and J. Ye, Phys. Rev. Lett. **69**, 2411 (1992).
[29] P. Coleman and C. Pépin, Physica (Amsterdam) **312-313**, 383 (2002).
[30] Y. J. Uemura, T. Yamazaki, D. R. Harshman, M. Senba, and E. J. Ansaldo, Phys. Rev. B **31**, 546 (1985).

[31] A. Keren, P. Mendels, I. A. Campbell, and J. Lord, Phys. Rev. Lett. **77**, 1386 (1996).
[32] W. Lee, S. Lee, K.-Y. Choi, K.-J. Lee, B.-J. Kim, B. J. Suh, S. Shin, and T. Park, Phys. Rev. B **96**, 224433 (2017).
[33] A. J. Bray, Phys. Rev. Lett. **59**, 586 (1987).
[34] K. Binder and A. P. Young, Rev. Mod. Phys. **58**, 801 (1986).
[35] I. A. Campbell, A. Amato, F. N. Gygax, D. Herlach, A. Schenck, R. Cywinski, and S. H. Kilcoyne, Phys. Rev. Lett. **72**, 1291 (1994).
[36] J. G. Vale and E. C. Hunter, Phys. Rev. B **98**, 100406(R) (2018).